J|A|C|S
ARTICLES
Published on Web 06/27/2006

The Pb_{12}^{2-} and Pb_{10}^{2-} Zintl Ions and the $M@Pb_{12}^{2-}$ and $M@Pb_{10}^{2-}$ Cluster Series Where M = Ni, Pd, Pt

Emren N. Esenturk, James Fettinger, and Bryan Eichhorn*

Contribution from the Department of Chemistry and Biochemistry, University of Maryland, College Park, Maryland 20742

Received March 17, 2006; E-mail: eichhorn@umd.edu

Abstract: Ethylenediamine (en) solutions of K_4Pb_9 react with toluene solutions of ML_4 (M = Pt, Pd, L = PPh_3; M = Ni, L_2 = COD) and 2,2,2-crypt to give $M@Pb_{12}^{2-}$ cluster anions (M = Pt (1), Pd (2), Ni (3)) as the $[K(2,2,2\text{-crypt})]^+$ salts in low (Ni) to good (Pt) yields. The ions have near perfect I_h point symmetry and have been characterized by X-ray diffraction, ^{207}Pb NMR and LDI-TOF mass spectrometry studies. For M = Ni, the primary product formed is the D_{4d} $Ni@Pb_{10}^{2-}$ cluster that has also been structurally characterized. The $M@Pb_{10}^{2-}$ clusters (M = Pd, Pt) and the new Zintl ions *closo*-Pb_{10}^{2-} and *closo*-Pb_{12}^{2-} were formed in the gas phase but have not been detected in solution or the solid state. The structural trends of these series of clusters have been investigated through DFT calculations. The $Ni@Pb_{10}^{2-}$ cluster is dynamic on the ^{207}Pb NMR time scale at −45 °C and 104.7 MHz. The $M@Pb_{12}^{2-}$ ions show unusually deshielded ^{207}Pb NMR chemical shifts that presumably arise from σ-aromatic effects associated with their high symmetries. In the solid state, the salts form superlattices of cations and anions (e.g. the AlB_2 lattice of $[K(2,2,2\text{-crypt})]_2[Pt@Pb_{12}]$) and are prototypes for "assembled cluster materials".

Introduction

The controlled aggregation of clusters into ordered arrays of "assembled cluster materials" (ACMs) with novel properties has been a long-term goal of cluster science research.[1] To optimize cooperative effects between clusters in the solid state, small intercluster separations and regular packing of components must be achieved—preferably through self-assembly. The field of functional nanoparticles serves as a guide in this regard in that composite materials formed from their assemblies often have remarkable properties. For example, the CdTe/CdSe nanocrystalline composite solar cell[2] was prepared by depositing alternating layers of CdTe and CdSe nanoparticles from colloidal suspensions and shows distinct advantages over bulk and organic thin film devices. The ability to precisely control composition, size, and anisotropy through molecular cluster synthesis provides an advantage over nanoparticle (NP) materials where some dispersity in size and composition is unavoidable and chemical anisotropy is often difficult to control.

To enhance intercluster cooperative phenomena, it is desirable to minimize or eliminate the stabilizing ligands to maximize intercluster contacts. This requirement is problematic in that unligated clusters are typically not stable and tend to coalesce into larger particles and bulk materials. The few examples of known ligand-free "magic clusters" are the exceptions to this problem because their inherent electronic stability precludes coalescence and, in theory, should allow for the formation of ACMs. The fullerene ACMs are the prototypes of stable, assembled clusters that self-assemble into novel materials. For example, C_{60} self-assembles into a close-packed matrix that, upon doping with alkali metals, forms superconducting ACMs with relatively high T_c's.[3,4]

Aside from the fullerene family, three other well-studied examples of ligand-free clusters are known, namely, the metallocarbohedrene family of M_8C_{12} cages (i.e. the "metcars" where M = transition metal),[5] the Al_{13}^{1-}- type centered icosahedra (i.e., $Al@Al_{12}^{1-}$),[6] and the growing class of naked Zintl ions and their derivatives.[7−9] Aside from the fullerenes, only the Zintl ions have been isolated in bulk form and have been crystallized as salts in well-ordered lattices. In some instances, cooperative effects between clusters can be enhanced through ionic bonding (e.g. the magnetic chains of MAs_8^{3-} ions linked by K^+ ions).[10]

Despite the vast potential of ACMs, materials prepared from assemblies of clusters are virtually unknown due to the paucity of naked cluster building blocks available. Further advancement of the ACM field will require bulk-phase synthesis of new ligand-free, "magic clusters" with controllable properties. Recent advances in the synthesis and characterization of naked bimetallic Zintl ions suggest that a wide variety of ligand-free, stable cluster ions may be accessible. The recent reports of bimetallic

(1) Seifert, G. *Nature* **2004**, *3*, 77.
(2) Gur, I.; Fromer, N. A.; Geier, M. L.; Alivisatos, A. P. *Science* **2005**, *310*, 462.
(3) Kraetschmer, W.; Lamb, L. D.; Fostiropoulos, K.; Huffman, D. R. *Nature* **1990**, *347*, 354.
(4) Kroto, H. W.; Heath, J. R.; Obrien, S. C.; Curl, R. F.; Smalley, R. E. *Nature* **1985**, *318*, 162.
(5) Guo, B. C.; Kerns, K. P.; Castleman, A. W. *Science* **1992**, *255*, 1411.
(6) Rubio, A.; Balbas, L. C.; Alonso, J. A. *Phys. B* **1991**, *168*, 32.
(7) Esenturk, E. N.; Fettinger, J.; Eichhorn, B. *Chem. Commun.* **2005**, 247.
(8) Esenturk, E. N.; Fettinger, J.; Lam, Y. F.; Eichhorn, B. *Angew. Chem., Int. Ed.* **2004**, *43*, 2132.
(9) Moses, M.; Fettinger, J.; Eichhorn, B. *Science* **2003**, *300*, 778.
(10) Kesanli, B.; Fettinger, J.; Eichhorn, B. W. *J. Am. Chem. Soc.* **2003**, *125*, 7367.

10.1021/ja061842m CCC: $33.50

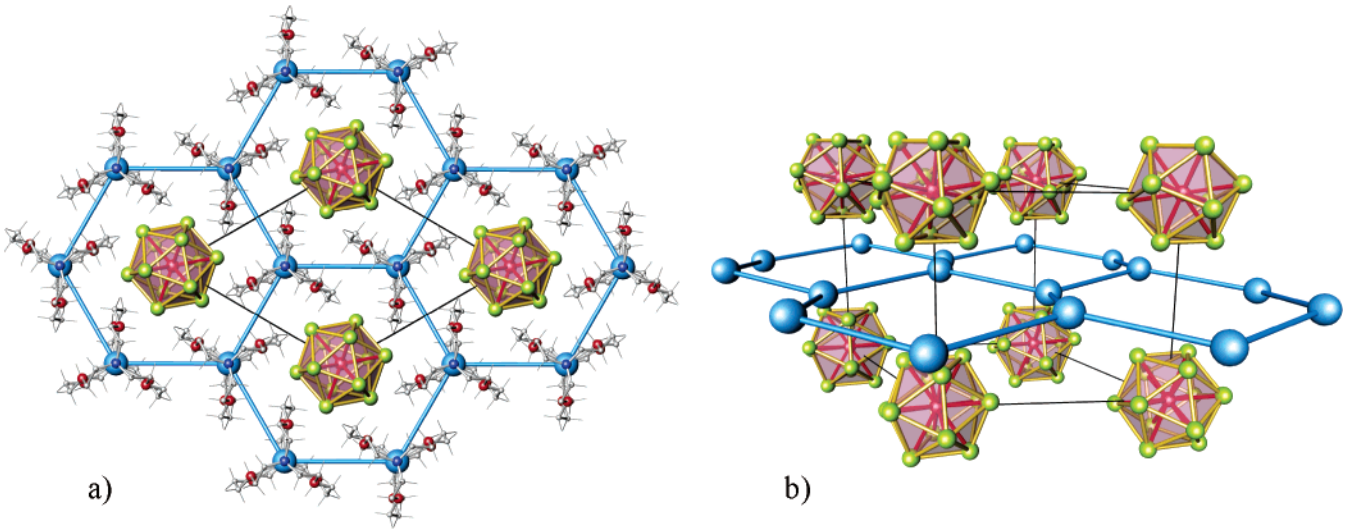

Figure 1. (a) 001 projection of the $[K(2,2,2\text{-crypt})]_2[Pt@Pb_{12}]$ structure showing the polyhedral anions and cations on $\bar{3}$ inversion and three-fold rotation axes, respectively, in an AlB_2 type lattice. The lines joining the K^+ ions are a guide to the eye to illustrate the hexagonal network but do not represent bonds. (b) Perspective showing the $Pt@Pb_{12}^{2-}$ icosahedra above and below the puckered hexagonal net of K^+ ions. Pt is red (large), Pb is green, K is blue, C is gray, and O is red (small).

clusters (e.g., Ni_2Sn_{17},[4−] $PtPb_{12}^{2-}$, $AlPb_{12}^{+}$)[8,11,12] and metalloid clusters (e.g., $As@Ni_{12}@As_{21}^{3-}$, Pd_2Ge_{18},[4−] $Ni_3@Ge_{18}$,[4−] Pd_7As_{16}[4−])[9,13−15] are examples of such species. Recent theoretical studies have been used to target new clusters with potentially interesting properties, such as the E_{12}^{4-} and the E_{10}^{2-} ions (E = Si, Ge, Sn, Pb) and their metal-centered derivatives.[16−23] However, experimental data on these bimetallic systems are limited, and the naked ions were unknown prior to our studies.[12,24,25] We report here (1) the synthesis, structures, and properties of two series of ligand-free bimetallic clusters; $M@Pb_{12}^{2-}$ and $M@Pb_{10}^{2-}$ where M = Ni, Pd, Pt and (2) the gas-phase identification of two new deltahedral Zintl anions, *closo*-Pb_{10}^{2-} and *closo*-Pb_{12}^{2-}. Preliminary communications of the $Pt@Pb_{12}^{2-}$ and $Ni@Pb_{10}^{2-}$ anions have been reported.[7,8]

Synthesis. Ethylenediamine (en) solutions of K_4Pb_9 react with toluene solutions of ML_4 (M = Pt, Pd, L = PPh_3; M = Ni, L_2 = COD) in the presence of 4 equiv of 2,2,2-crypt to give $[M@Pb_{12}]^{2-}$ cluster anions (M = Pt (**1**), Pd (**2**), Ni (**3**)) as the $[K(2,2,2\text{-crypt})]^+$ salts. The salts crystallize in very low (Ni, ∼2%) to good yields (Pt, 60%; Pd, 36%) and have been characterized by single-crystal XRD, energy dispersive X-ray (EDX) analysis, ^{207}Pb NMR, ^{195}Pt NMR (for anion **1**), and laser desorption/ionization-time-of-flight mass spectrometry (LDI-TOF MS). The salts form as dark-brown, blocklike crystals (Pt) or thin, red-brown plates (Pd and Ni) that are soluble in DMF, CH_3CN, and DMSO and are very air and moisture sensitive in solution and in the solid state.

The formation of the cluster anions requires a net oxidation of the starting materials that is accompanied by a reduction of the displaced ligands as shown in eqs 1 and 2.

$$4\ Pb_9^{4-} + 3\ M(PPh_3)_4 \xrightarrow[\text{en/tol}]{\text{2,2,2-crypt}} 3\ MPb_{12}^{2-} + 7\ PPh_3 + 5\ Ph_2P^{-1} + 5\ Ph^- \quad M = Pt(\mathbf{1}),\ Pd\ (\mathbf{2}) \quad (1)$$

$$4\ Pb_9^{4-} + 3\ Ni(C_8H_{12})_2 + 10\ NH_2(CH_2)_2NH_2 \xrightarrow{\text{2,2,2-crypt}} 3\ NiPb_{12}^{2-} + 5\ C_8H_{14} + C_8H_{12} + 10\ NH_2(CH_2)_2NH^{1-} \quad (\mathbf{3}) \quad (2)$$

In reaction 1, the phenyl and Ph_2P^{1-} byproducts were identified by GC−MS and ESI-MS studies and ^{31}P NMR spectroscopy. The reductive decomposition of the PPh_3 ligand is directly analogous to the well-known reductive cleavage of PPh_3 by alkali metals to give alkali-PPh_2 salts and biphenyl (or NaPh).[26] For reaction 2, the en solvent molecules are formally reduced with the generation of H_2 and $NH_2(CH_2)_2NH^{1-}$ ions. The eliminated equivalents of H_2 are trapped through the hydrogenation of COD to form cyclooctene, which was identified in the reaction mixture by GC−MS analysis.

While the $Ni@Pb_{12}^{2-}$ ion is reproducibly formed from the reaction of $Ni(C_8H_{12})_2$ and Pb_9^{4-} (eq 2), the major product of this reaction is $Ni@Pb_{10}^{2-}$ (**4**). The $[K(2,2,2\text{-crypt})]^+$ salts of **3** and **4** are very similar in appearance (thin, red-brown plates) and difficult to differentiate in the solid state. They are formed competitively in a ca. 1:9 ratio (**3**:**4**) as estimated from ^{207}Pb NMR analysis (see NMR section). The Pt and Pd analogues of $Ni@Pb_{10}^{2-}$ have not been identified in the solid state or in solution; however, they do form in the gas phase and have been unequivocally identified by ESI-MS (see Mass Spectrometry section).

(11) Esenturk, E. N.; Fettinger, J.; Eichhorn, B. *J. Am. Chem. Soc.* **2006**, *128*, 12.
(12) Neukermans, S.; Janssens, E.; Chen, Z. F.; Silverans, R. E.; Schleyer, P. V.; Lievens, P. *Phys Rev. Lett.* **2004**, *92*, 163401−1.
(13) Goicoechea, J. M.; Sevov, S. C. *J. Am. Chem. Soc.* **2005**, *127*, 7676.
(14) Goicoechea, J. M.; Sevov, S. C. *Angew. Chem., Int. Ed.* **2005**, *44*, 4026.
(15) Moses, M.; Fettinger, J.; Eichhorn, B. 2006. Manuscript submitted.
(16) Hagelberg, F.; Xiao, C.; Lester, W. A. *Phys. Rev. B* **2003**, *67*, 035426−1.
(17) Kumar, V.; Kawazoe, Y. *App. Phys. Lett.* **2002**, *80*, 859.
(18) Kumar, V.; Kawazoe, Y. *App. Phys. Lett.* **2003**, *83*, 2677.
(19) Kumar, V.; Singh, A. K.; Kawazoe, Y. *Nano Lett.* **2004**, *4*, 677.
(20) Lu, J.; Nagase, S. *Phys. Rev. Lett.* **2003**, *90*, 115506−1.
(21) Lu, J.; Nagase, S. *Chem. Phys. Lett.* **2003**, *372*, 394.
(22) Sen, P.; Mitas, L. *Phys. Rev. B* **2003**, *68*, 155404.
(23) Sun, Q.; Wang, Q.; Briere, T. M.; Kumar, V.; Kawazoe, Y.; Jena, P. *Phys. Rev. B* **2002**, *65*, 235417.
(24) Hiura, H.; Miyazaki, T.; Kanayama, T. *Phys. Rev. Lett.* **2001**, *86*, 1733.
(25) Zhang, X.; Li, G. L.; Xing, X. P.; Zhao, X.; Tang, Z. C.; Gao, Z. *Rapid Commun. Mass Spectrom.* **2001**, *15*, 2399.
(26) Gee, W.; Shaw, R. A.; Smith, B. C.; Bullen, G. J. *J. Chem. Soc.* **1964**, 4180.

Table 1. Crystallographic Data for the $M@Pb_{12}^{2-}$ (M = Pt, Pd, Ni) Salts

	$[PtPb_{12}][K(2,2,2\text{-crypt})]_2$	$[PdPb_{12}][K(2,2,2\text{-crypt})]_2 \cdot tol$	$[NiPb_{12}][K(2,2,2\text{-crypt})]_2 \cdot en$
empirical formula	$PtPb_{12}C_{36}H_{72}K_2N_4O_{12}$	$PdPb_{12}C_{43}H_{80}K_2N_4O_{12}$	$NiPb_{12}C_{38}H_{80}K_2N_6O_{12}$
formula weight	3512.55	3515.99	3436.17
temperature (K)	173(2)	173(2)	173(2)
wavelength (Å)	0.71073	0.71073	0.71073
crystal system	trigonal	triclinic	triclinic
space group	$P\bar{3}$	$P\bar{1}$	$P\bar{1}$
unit cell dimensions			
a (Å)	13.041(6)	13.5900(11)	14.566(4)
b (Å)	13.041(6)	13.9389(11)	15.469(5)
c (Å)	11.672(11)	22.1236(17)	16.400(5)
α (deg)	90	72.1144(15)	62.914(5)
β (deg)	90	85.2884(16)	64.289(5)
γ (deg)	120	64.1532(15)	87.127(5)
volume (Å^3)	1719.1(19)	3582.8(5)	2913.8(15)
Z	1	2	2
D_{calcd} (Mg/m^3)	3.393	3.259	2.427
abs coeff (mm^{-1})	31.448	28.485	17.622
goodness of fit on F^2	1.055	0.996	1.013
final *R* indices [$I > 2\sigma(I)$][a]			
R1	0.0352	0.0596	0.1199
wR2	0.0825	0.1560	0.2976
R indices (all data)[a]			
R1	0.0730	0.1014	0.2025
wR2	0.0959	0.1671	0.3289

[a] The function minimized during the full-matrix least-squares refinement was $\sum w(F_o^2 - F_c^2)$ where $w = 1/[\sigma^2(F_o^2) + (0.0380*P)2 + 5.4664*P]$ and $P = \max(F_o^2,0)+(2*F_c^2)/3$.

Solid State Structures. The $[K(2,2,2\text{-crypt})]^+$ salts of the $M@Pb_{12}^{2-}$ (M = Pt, Pd, Ni) anions have been structurally characterized by single crystal X-ray diffraction. The cations and anions have three-fold rotation axes, but this symmetry is only crystallographically imposed in the $Pt@Pb_{12}^{2-}$ structure. The $[K(2,2,2\text{-crypt})]_2[Pt@Pb_{12}]$ salt is trigonal, space group $P\bar{3}$, with the $Pt@Pb_{12}^{2-}$ anion and the $[K(2,2,2\text{-crypt})]^+$ cations located on $\bar{3}$ inversion and three-fold rotation axes, respectively (see Figure 1). The $[K(2,2,2\text{-crypt})]_2[M@Pb_{12}]\cdot$solvent crystals (M = Pd and Ni, solvent = toluene and ethylenediamine, respectively) are both triclinic, space group $P\bar{1}$, but are not isomorphic. Both sets of crystals were plagued by twinning, and the Ni derivative was also highly disordered. While the twinning was successfully treated in both cases, the disorder in the Ni structure resulted in high *R*-factors that limit the accuracy and precision of the metric parameters. However, the general structures are unequivocal.

Each lattice contains noninteracting $M@Pb_{12}^{2-}$ icosahedra with two $[K(2,2,2\text{-crypt})]^+$ cations. The solvent molecules in the Ni and Pd structures do not significantly interact with anions or cations. The Pt and Pd clusters are well ordered in their respective lattices despite their almost spherical nature (cf. C_{60}). A summary of the crystallographic data is given in Table 1. Bond distances and angles for the clusters are given in Tables S-1 and S-2 of the Supporting Information.

The $M@Pb_{12}^{2-}$ anions are defined by 12 Pb atoms that form icosahedral cages with transition metals (Pt, Pd, Ni) at the center. The $Pt@Pb_{12}^{2-}$ anion displays near perfect I_h point symmetry, whereas the Pd and Ni centered anions are slightly distorted. The $Pd@Pb_{12}^{2-}$ anion is shown in Figure 2 as an example. A comparative summary of metric parameters for the three ions is given in Table 2. The Pb−Pb contacts for the three anions (3.019(4) − 3.23(4) Å) are in the low end of the range of the other structurally characterized polyplumbide clusters,

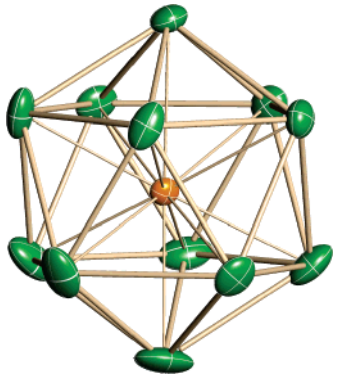

Figure 2. ORTEP drawing of the $Pd@Pb_{12}^{2-}$ ion. Pd is orange, Pb is green, thermal ellipsoids are set at the 50% probability level.

$[MPb_9(CO)_3]^{4-}$ (M = Cr, Mo, W)[27,28] Pb_9^{4-},[29] Pb_9^{3-},[30] and Pb_5^{2-},[31] where the distances vary between 3.03 and 3.41 Å.

Although the quality of the $Ni@Pb_{12}^{2-}$ structure is of low resolution, the bond distances and degree of distortion in the anions **1**, **2**, and **3** appear to vary according to the atomic radius of the centered transition metal atom. As the atom becomes smaller, the Pb−Pb, Pb−M, and icosahedral diagonal distances decrease as expected (Table 2). In addition, the range and variance of Pb−Pb and Pb−M contacts increase with the decreasing size of M, which suggests that the Pb_{12} framework distorts when an atom smaller that Pt is inserted in the center. For example, $Pt@Pb_{12}^{2-}$ has a very narrow 0.028 Å range of Pb−Pb bond distances with a remarkably small variance (1.4×10^{-4}). In comparison, the Pb−Pb contacts for **2** and **3** are shorter with larger distributions of distances. The range of

(27) Eichhorn, B. W.; Haushalter, R. C. *J. Chem. Soc., Chem. Commun.* **1990**, 937.
(28) Campbell, J.; Mercier, H. P. A.; Franke, H.; Santry, D. P.; Dixon, D. A.; Schrobilgen, G. J. *Inorg. Chem.* **2002**, *41*, 86−107.
(29) Campbell, J.; Dixon, D. A.; Mercier, H. P. A.; Schrobilgen, G. J. *Inorg. Chem.* **1995**, *34*, 5798−5809.
(30) Fassler, T. F.; Hunziker, M. *Inorg. Chem.* **1994**, *33*, 5380.
(31) Edwards, P. A.; Corbett, J. D. *Inorg. Chem.* **1977**, *16*, 903.

Table 2. Summary of Structural Data for the M@Pb_{12}^{2-} (M = Pt, Pd, Ni) Anions

			Pb–M distances			Pb–Pb distances		
metal (M)	covalent radii of M (Å)[a]	diagonal distance (av) (Å)	average (Å)	range (Å)	variance[b] $\sigma^2 \times 10^{-3}$	average (Å)	range (Å)	variance[b] $\sigma^2 \times 10^{-3}$
Pt	1.36	6.116(6)	3.058(7)	0.003	0.0044	3.216(12)	0.028	0.14
Pd	1.35	6.067(5)	3.033(7)	0.112	1.1	3.189(9)	0.080	0.33
Ni	1.22	5.983(4)	3.001(24)	0.112	1.3	3.078(9)	0.214	3.1

[a] Data from ref 32. [b] Variance is defined as: $\sigma^2 = [\sum_{i=1}^{N} (x_i - \bar{x})^2]/(N-1)$.

Pb−M contacts can also be used as indicators of the "fit" of the centered metal atom and are larger for Ni and Pd (0.112 Å) relative to Pt (0.003Å). These data depict a highly isotropic Pt@Pb_{12}^{2-} cluster with almost no distortion, whereas the Ni@Pb_{12}^{2-} and Pd@Pb_{12}^{2-} ions reveal structural anisotropy that may signal cluster instability. This structural instability is consistent with the Ni@Pb_{12}^{2-} and Ni@Pb_{10}^{2-} product distribution in which Ni favors the 10-atom cluster relative to the icosahedron. The distortions and cluster size effects are discussed in the Computational section.

The M@Pb_{12}^{2-} clusters are 12-vertex, 26-electron polyhedra with highly regular *closo* icosahedral structures as predicted from a Wade−Mingos analysis.[33] In this analysis, the Pb atoms donate two electrons each to cluster bonding, and the centered Pt, Pd, and Ni atoms donate zero electrons to give 26-electron, $2n+2$ *closo* clusters when the −2 charge is taken into consideration. An alternative cluster electron-counting scheme, the topological electron count theory introduced by Teo,[34] classifies clusters according to the number of skeletal electron pairs. The number of skeletal electron pairs are determined by the equation, $B = N/2 - (V_n + 6V_m)$, where N is number of total cluster valence electrons, V_n is number of surface main group atoms and V_m is number of surface transition metal atoms. For the anions **1**, **2**, and **3**, $N = 10\ e^-$ (Pt, Pd or Ni) + $12 \times 4\ e^-$ (Pb) + $2\ e^-$ (charge) = $60\ e^-$. Therefore, $B = 60/2 - (12 + 6 \times 0) = 18$ pair e^-, which is considered as characteristic of electron-rich icosahedral clusters and common for transition-metal centered species.[34]

The Ni@Pb_{10}^{2-} anion crystallizes with two $[K(2,2,2\text{-crypt})]^+$ cations in the monoclinic system, space group $C2/c$. Summaries of the crystallographic data and selected bond distances and angles for the complex are given in Tables 3 and 4, respectively. The anion possesses virtual D_{4d} point symmetry and is defined by a 10-vertex Pb_{10}^{2-} bicapped square antiprism centered by a Ni atom (Figure 3). According to the conventions for Wade's rules for electron counting,[33] it is a 22-electron, $2n+2$ framework with a *closo* geometry when the −2 charge of the cluster is taken into consideration. The two axial Pb−Ni bonds are elongated (3.210(3) Å (av)) in comparison with the other eight Pb−Ni bonds in the complex (2.722(2) Å). The 24 Pb−Pb contacts of the Pb_{10} deltahedron can be categorized into three different types. The average distances to the capping Pb atom (Pb1) are the shortest at 3.094(2) Å. The Pb−Pb contacts between square planes are intermediate at 3.135(3) Å (av), whereas the distances within the square planes are longest at 3.405(2) Å (av). A recent theoretical study by Schrodt et al. of stable, binary metal atom clusters suggested that the neutral, bicapped, tetragonal, antiprism anion, $Pb_{10}Ni$, with D_{4d} point symmetry is the most stable isomer compared to other isomers.[35] Their DFT calculations predicted Pb−Pb bond distances of 3.12−3.21 Å and Pb−Ni distances of 2.89−2.99 Å that are reasonably close to the experimental results reported here. The discrepancies presumably result from the differences in charge between the model and the isolated cluster, which finds the latter in a more axially elongated structure. The structures of the Pt- and Pd-centered clusters have been evaluated though DFT modeling and are discussed in the DFT modeling section.

Table 3. Crystallographic Data for $[NiPb_{10}][K(2,2,2\text{-crypt})]_2$

empirical formula	$NiPb_{10}C_{36}H_{72}K_2N_4O_{12}$
formula weight	2961.79
temperature (K)	173(2)
wavelength (Å)	0.71073
crystal system	monoclinic
space group	$C2/c$
unit cell dimensions	
a (Å)	25(2)
b (Å)	11.940(4)
c (Å)	21.400(2)
α (deg)	90
β (deg)	96.91
γ (deg)	90
volume (Å^3)	6304(507)
Z	4
D_{calcd} (Mg/m^3)	3.120
data/restraints/parameters	5758/0/295
goodness of fit on F^2	1.060
final R indices [$I > 2\sigma(I)$][a]	
R1	0.0582
wR2	0.1645
R indices (all data)[a]	
R1	0.0827
wR2	0.1764

[a] The function minimized during the full-matrix least-squares refinement was $\sum w(F_o^2 - F_c^2)$ where $w = 1/[\sigma^2(F_o^2) + (0.0380*P)^2 + 5.4664*P]$ and $P = \max(F_o^2,0) + (2*F_c^2)/3$.

Table 4. Selected Bond Lengths [Å] and Angles [deg] for the Ni@Pb_{10}^{2-} Ion

Ni(1)−Pb(1)	3.210(1)	Pb(1)−Pb(2)	3.103(1)
Ni(1)−Pb(2)	2.717(1)	Pb(2)−Pb(3)	3.445(1)
Ni(1)−Pb(3)	2.720(2)	Pb(2)−Pb(3′)	3.130(1)
Ni(1)−Pb(4)	2.716(1)	Pb(3)−Pb(4)	3.411(1)
Ni(1)−Pb(5)	2.733(2)	Pb(4)−Pb(2′)	3.141(1)
Pb(1)−Ni(1)−Pb(1′)	179.59(8)	Pb(1)−Pb(3)−Pb(4)	55.89(2)
Pb(2)−Ni(1)−Pb(3)	78.65(5)	Pb(1)−Pb(3)−Pb(2′)	109.00(2)
Pb(3′)−Ni(1)−Pb(1)	117.78(6)	Ni(1)−Pb(2)−Pb(1)	66.56(2)
Pb(4)−Ni(1)−Pb(1)	61.67(2)	Pb(4)−Pb(1)−Pb(2)	102.15(2)
Pb(4)−Ni(1)−Pb(2)	124.14(2)	Pb(4)−Pb(1)−Ni(1)	51.21(2)
Pb(4)−Ni(1)−Pb(4′)	138.92(9)	Pb(5)−Pb(4)−Pb(3)	90.80(2)

Mass Spectrometry Studies. The laser desorption ionization time-of-flight (LDI-TOF) mass spectra for the M@Pb_{12}^{2-} (M = Pt, Pd, Ni) ions were recorded in the negative ion mode. The spectra were recorded from pure samples of the [K(2,2,2-

(32) Pauling, L. *Proc. Natl. Acad. Sci. U.S.A.* **1975**, *72*, 3799.
(33) Wade, K. *Adv. Inorg. Chem. Radiochem.* **1976**, *18*, 1.
(34) Zhang, H.; Teo, B. K. *Inorg. Chim. Acta* **1997**, *265*, 213.
(35) Schrodt, C.; Weigend, F.; Ahlrichs, R. *Z. Anorg. Allg. Chem.* **2002**, *628*, 2478.

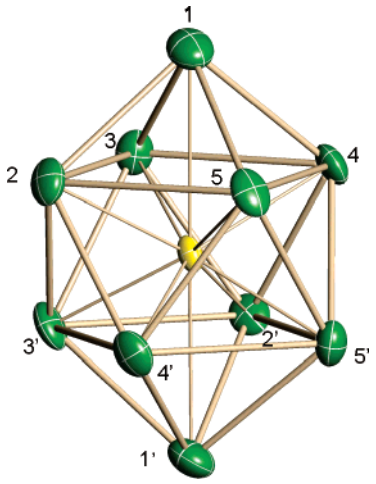

Figure 3. ORTEP drawing of the $Ni@Pb_{10}^{2-}$ ion showing bicapped, square antiprismatic structure. Ni is yellow, Pb is green. Thermal ellipsoids are set at the 50% probability level.

crypt)]$_2$[M@Pb_{12}] (M = Pt, Pd, Ni) crystals that were dissolved in DMF and deposited on carbon tape on the LDI-MS sample holder. The spectrum of [K(2,2,2-crypt)]$_2$[Pt@Pb_{12}] is shown in Figure 4 as an example. The spectra show strong signals of the $M@Pb_{12}^{1-}$ (M = Pt, Pd, Ni) monoanions with mass envelopes arising from the multiple isotopes of Pb and M of the respective compounds. The inset of Figure 4 shows the observed and simulated mass envelopes for $Pt@Pb_{12}^{2-}$. The calculated and observed peaks for $M@Pb_{12}^{2-}$ (M = Pd, Ni) are quite similar and are given in the Supporting Information (Figure S1). In addition to the parent ion, each of the spectra shows strong signals for the empty Pb_{12}^{1-} and Pb_{10}^{1-} ions, the metal-centered $M@Pb_{10}^{1-}$ cluster and the K^+-coordinated ion pairs for all (see Figure 4 as an example). The data are important for the following reasons. (1) The K^+ ion pairs shows that the native clusters all carry a −2 charge as expected from electron-counting considerations, (2) the parent Pb_{12}^{2-} and Pb_{10}^{2-} ions (Figure 5 a, b) represent the first experimental proof of the elusive[36−38] E_{12} and E_{10} naked cluster anions, and (3) the data show that the M = Pt and Pd derivatives of the $M@Pb_{10}^{2-}$ clusters are stable enough to exist in the gas phase (Figure 5c, Figure 4) even though neither has been detected in solution or the solid state.

The Pb_{12}^{2-} and Pb_{10}^{2-} ions, as well as the metalated $M@Pb_{10}^{-2}$ ions, apparently form from the fragmentation of the $M@Pb_{12}^{-2}$ anions during the LDI process since the LDI-MS data were obtained from salts of the [K(2,2,2-crypt)]$_2$[M@Pb_{12}] crystals. Note that the Pb_{12}^{2-}, Pb_{10}^{2-}, $Pt@Pb_{10}^{2-}$, and $Pd@Pb_{10}^{2-}$ clusters have not been detected in solution or in the solid state. The calculated and observed mass envelopes for the Pb_{12}^{2-} and Pb_{10}^{2-} ions are shown in Figure 5. DFT studies indicated that all have the expected $2n+2$ *closo* structures and are similar to the structurally characterized metalated derivatives (see next section). It is interesting to note the *relative* peak intensity of the KPb_{12}^{2-} ion is larger than that of the other potassium-coordinated complexes (Figure 4). This anomaly may arise from the ability of the K^+ ion to reside inside the Pb_{12}^{2-} cluster, which would give rise to added stability in the ion pair.

DFT Studies. DFT calculations have been performed on the Pb_{12}^{2-} and Pb_{10}^{2-} ions as well as the $M@Pb_{10}^{2-}$ (M = Ni, Pd, Pt) anions to compare and contrast with structural data and evaluate the structural evolutions that occur with the centering of a metal. Theoretical studies of neutral $M@Pb_{10}$ and $M@Pb_{12}$ clusters as well as selected $M@E_{12}$ icosahedral clusters ions (M = Cu, Zn, Cd; E = Si, Ge, Sn) have been reported elsewhere.[16,17] However, a systematic study of structural trends in the present series and correlations with structural data has not been previously described.

The electronic structures of the $M@E_{12}^{2-}$ icosahedral clusters are unusual in view of their high I_h point symmetry in which the five d-orbitals of the centered transition metal transform together under the h_g irreducible representation.[8] This five-fold degeneracy is reminiscent of the gas-phase electronic structures of the isolated atoms and is not encountered elsewhere in molecular chemistry. In addition, the high symmetry gives rise to a highly delocalized, three-dimensional σ-bonding network. A resulting σ-aromatic character has been described in detail elsewhere[39−41] for this class of clusters. The ramifications of this delocalized bonding are described in the NMR section below.

The program package PRIRODA[42,43] was used for DFT calculations with SBK effective core potentials and 311-split basis sets for the Pb atoms. The Pb_{10}^{2-} and $M@Pb_{10}^{2-}$ ions have a bicapped, square antiprismic structure with D_{4d} point symmetry. The X-ray structure for the $Ni@Pb_{10}^{2-}$ anion was used as the starting geometry for all four anions. The starting geometries were then optimized, and the calculated metric parameters are summarized in Table 5 along with the crystallographic data for $Ni@Pb_{10}^{2-}$. The calculated bond distances are ∼0.05 Å longer than the crystallographically observed distances for $Ni@Pb_{10}^{2-}$, presumably due to lack of inclusion of cations in the calculations. However, the agreement between calculated and observed structural data for $Ni@Pb_{10}^{2-}$ is excellent, suggesting that the calculated structural data for the remaining ions are reliable.

Several interesting trends emerge from Table 5. First, the trends in Pb−Pb distances within each cluster are consistent with the crystallographically observed trends for all the E_9 clusters.[44−48] In these systems, E−E contacts to the 4-coordinate cap are the shortest whereas the E−E distances within the square planes are the longest. Second, the metric parameters of the empty Pb_{10}^{2-} ion are very similar to the calculated and observed distances of $Ni@Pb_{10}^{2-}$, suggesting that Pb_{10} framework is virtually undistorted when a Ni atom is incorporated at the center. In contrast, the average Pb−Pb distances of the Pd and Pt systems increase systematically as the atomic radius of the central atom increases. This trend suggests that the Pb_{10} framework is stretched beyond its preferred equilibrium size with the centering of these atoms. The average Pb−Pb contact

(36) Chen, Z.; Hirsch, A.; Nagase, S.; Walter, T.; Schleyer, P. V. *J. Am. Chem. Soc.* **2003**, *125*, 15507.
(37) Schleyer, P. V.; Jiao, H. *Pure Appl. Chem.* **1996**, *68*, 209.
(38) Wang, J.; Wang, G.; Zhao, J. *Phys. Rev. B.* **2001**, *64*, 205411.
(39) Heine, T.; Schleyer, P. V.; Corminboeuf, C.; Seifert, G.; Reviakine, R.; Weber, J. *J. Phys. Chem. A* **2003**, *107*, 6470.
(40) King, R. B.; Heine, T.; Corminboeuf, C.; Schleyer, P. V. *J. Am. Chem. Soc.* **2004**, *126*, 430.
(41) Schleyer, P. V.; Maerker, C.; Dransfeld, A.; Jiao, H.; Hommes, N. J. R. v. E. *J. Am. Chem. Soc.* **1996**, *118*, 6317.
(42) Nicolau, Y. F.; Dupuy, M.; Brunel, M. *J. Electrochem Soc* **1990**, *137*, 2915.
(43) O'Brien, P.; Nomura, R. *J. Mater. Chem.* **1995**, *5*, 1761.
(44) Corbett, J. D.; Edwards, P. A. *J. Am. Chem. Soc.* **1977**, *99*, 3313.
(45) Fassler, T. F.; Hoffmann, R. *Angew. Chem., Int. Ed.* **1999**, *38*, 543.
(46) Fassler, T. F.; Schutz, U. *Inorg. Chem.* **1999**, *38*, 1866.
(47) Queneau, V.; Sevov, S. C. *Angew. Chem., Int. Ed. Engl.* **1997**, *36*, 1754.
(48) Todorov, E.; Sevov, S. C. *Inorg. Chem.* **1998**, *37*, 3889.

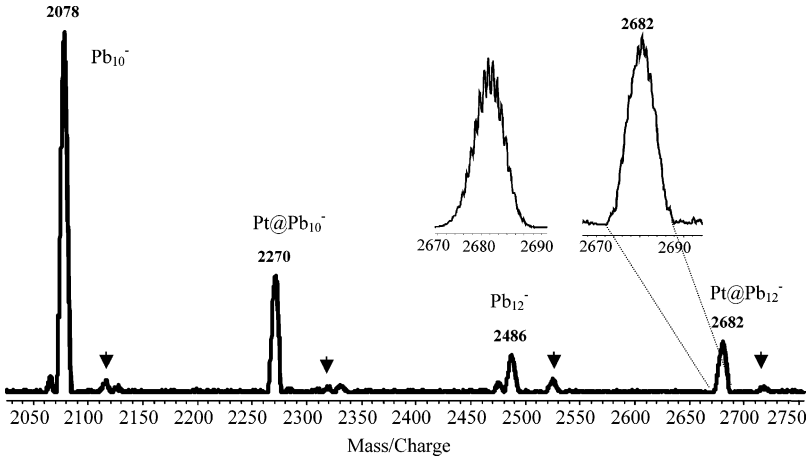

Figure 4. LDI-TOF mass spectra for $[K(2,2,2\text{-crypt})]_2[Pt@Pb_{12}]$ crystals. Arrows denote the potassium-coordinated ion pairs. (Inset)Enlarged view of the $Pt@Pb_{12}^-$ mass envelope along with its simulated pattern.

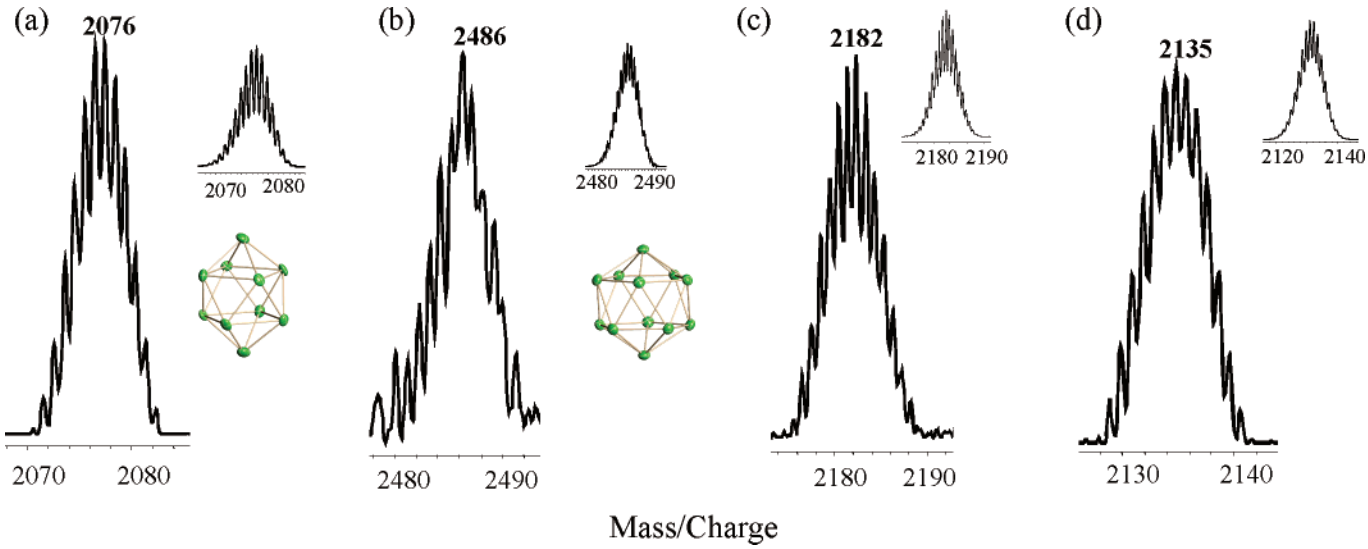

Figure 5. LDI-TOF mass spectrum of the (a) Pb_{12}^{-1}, (b) Pb_{10}^{-1}, (c) $Pd@Pb_{10}^{-1}$, (d) $Ni@Pb_{10}^{-1}$, ions. Calculated mass envelope of the corresponding ions and their proposed structures.

Table 5. Average Calculated Bond Lengths [Å] for $M@Pb_{10}^{2-}$ (M = Ni, Pd, Pt) and Empty Pb_{10}^{2-} Ions[a]

	Pt	Pd	Ni (calcd)	Ni (exptl)	Pb_{10}^{2-}
M−Pb Distances to Capping (Axial) Pb Atoms					
M−Pb(1)	3.256	3.276	3.266	3.210(1)	−
M−Pb Distances to Pb Atoms in the Square Planes					
M−Pb(2−5)	2.827	2.806	2.743	2.722(2)	−
All M−Pb Bonds					
average	2.913	2.900	2.848	2.820(9)	−
Pb−Pb Distances to the Capping (Axial) Pb Atoms					
Pb(1)−Pb(2−5)	3.158	3.155	3.123	3.094(2)	3.105
Pb−Pb Distances between the Square Planes					
Pb(2−5)−Pb(2′-5′)	3.266	3.249	3.177	3.135(3)	3.126
Pb−Pb Distances within the Square Planes					
Pb(2−5)−Pb(2−5)	3.533	3.501	3.422	3.405(2)	3.346
All Pb−Pb Bonds					
Average	3.310	3.290	3.225	3.192(4)	3.192

[a] See Figure 2 for numbering scheme.

increases by 0.12 Å in going from the empty Pb_{10}^{2-} cluster to $Pt@Pb_{10}^{2-}$, which is a destabilizing effect and is most likely responsible for the absence of the $Pd@Pb_{10}^{2-}$ and $Pt@Pb_{10}^{2-}$ in solution and in the solid state. Third, the expansion of the Pb_{10} cages due to centering is not isotropic. The short contacts within the square planes expand by 0.18 Å, whereas the distances to the capping Pb atoms change by only 0.06 Å. This anisotropic expansion is best illustrated in the trends of Pb−M distances. In the series, the average Pb−M distances to the Pb atoms in the square planes increase with increasing size of M, but the contacts to the axial Pb atoms actually decrease slightly. The latter presumably results from the forced expansion of the square planes, which draws the capping Pb atom closer to the transition metal to maintain reasonable Pb−Pb separations.

The $M@Pb_{12}^{2-}$ ions show similar trends in cluster distortions that result from size match/mismatch interactions between the centered metal atom and the Pb_{12} cluster. The calculated and observed $Pt@Pb_{12}^{2-}$ metric parameters are in excellent agreement (Table 6). Importantly, the calculated metric parameters for the empty Pb_{12}^{2-} ion are quite similar to the Pt-centered cluster and suggest that the Pt atom is best suited to be centered inside the Pb_{12} framework. The small Pd and Ni atoms result in a significantly contracted Pb_{12} framework, which presumably destabilizes the resulting clusters.

NMR Spectroscopic Studies. The ^{207}Pb NMR data for the $M@Pb_{12}^{2-}$ (M = Pt, Pd, Ni), $Ni@Pb_{10}^{2-}$ and Pb_9^{4-} cluster

Table 6. Calculated and Observed[a] Bond Lengths [Å] for M@Pb_{12}^{2-} and Empty Pb_{12}^{2-} Ions

Ni[a]	Pd[a]	Pt (obs)[a]	Pt (calc)	Pb_{12}^{2-} (calc)
Average M-Pb bonds				
3.00(2)	3.03(1)	3.06(1)	3.076	−
Average Pb−Pb bonds				
3.08(1)	3.19(1)	3.21(1)	3.234	3.213

[a] Crystallographic structural data from this study.

Table 7. ^{207}Pb NMR Chemical Shift Data[a]

anions	δ (ppm)[b]
$[Pt@Pb_{12}]^{2-}$ [(c)]	+1780
$[Pd@Pb_{12}]^{2-}$	+1520
$[Ni@Pb_{12}]^{2-}$	+1167
$[Ni@Pb_{10}]^{2-}$	−996
$[Pb_9]^{4-}$ [(d)]	−4098

[a] Recorded at 25 °C and 104.7 MHz. [b] Chemical shift versus $Pb(NO_3)_2$, 1 M in D_2O, $\delta = -2961.2$ ppm. [c] $^1J_{207_{Pb}-195_{Pt}} \approx 3440$ Hz. [d] Data from ref 49.

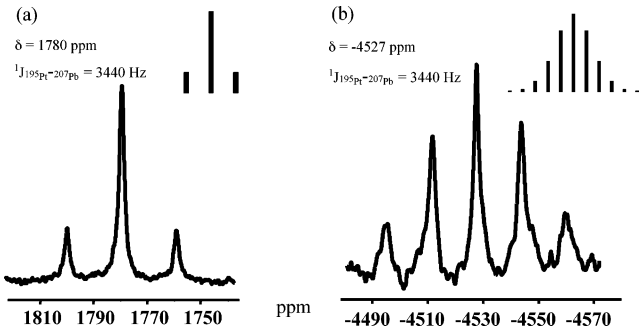

Figure 6. (a) ^{207}Pb NMR spectrum of $[Pt@Pb_{12}]^{2-}$ ion recorded in DMF at 11 °C and 83.7 MHz. (b) ^{195}Pt NMR spectrum of $[Pt@Pb_{12}]^{2-}$ ion recorded in DMF @ 11 °C and 107.5 MHz.

anions are summarized in Table 7. The ^{207}Pb NMR spectra for the M@Pb_{12}^{2-} ions each have a single resonance arising from the 12 chemically equivalent Pb atoms in the respective structures. While the Pd and Ni complexes give rise to simple singlets, the ^{207}Pb NMR spectrum for Pt@Pb_{12}^{2-} shows a singlet flanked by Pt satellites ($^1J_{207_{Pb}-195_{Pt}} \approx 3440$ Hz, 34% rel int, for ^{195}Pt, $I = {}^1/_2$, 34% abund.), indicating strong coupling to the central Pt atom (Figure 6a). The corresponding ^{195}Pt NMR spectrum (Figure 6b) shows a single resonance at −4527 ppm with a satellite pattern arising from coupling to 12 equivalent Pb atoms ($^1J_{207_{Pb}-195_{Pt}} \approx 3440$ Hz, for ^{207}Pb, $I = {}^1/_2$, 23% abund.). Both spectra are consistent with the nuclearity of the cluster and its solid-state structure. The measured ^{209}Pb NMR longitudinal relaxation time (T_1) for Pt@Pb_{12}^{2-} is quite short at 1.5 ms, which is over an order of magnitude shorter than the T_1 value of Pb_9^{4-} (39.8 ms) under identical conditions (DMF solvent, 11 °C, 107.5 MHz).

The M@Pb_{12}^{2-} ions have markedly downfield chemical shifts relative to other known lead compounds.[7,28,49] Typical lead compounds have chemical shifts in the rage of 0 to −4500 ppm, and most polyanions are in the upfield portion of this range (*cf.* Pb_9^{4-} at − 4098 ppm). The anomalous chemical shift may be due to the σ-aromatic character of the cluster arising from the novel electronic structure associated with the high I_h point symmetry. Chen, Schleyer, and King have described [12,40,41] this phenomenon in closely related hypothetical cluster species, but the magnitude and sign of aromaticity in the present compounds have not been reported to our knowledge. Support for assigning the downfield shift to σ-aromatic effects can be found in the comparison between the Ni@Pb_{10}^{2-} and Ni@Pb_{12}^{2-}, which have similar structures, charges, and nuclearities, but their ^{207}Pb NMR chemical shifts differ by more than 2000 ppm.

The bicapped, square pyramidal D_{4d} structure of Ni@Pb_{10}^{2-} has two chemically distinct lead environments, but its ^{207}Pb NMR spectrum shows a single, broad resonance at −996 ppm ($\Delta\nu_{1/2} = 280$ Hz, at 25 °C) due to dynamic exchange. For comparison, Pb_9^{4-} shows a relatively sharp resonance ($\Delta\nu_{1/2} = 47$ Hz, at 25 °C) under the same conditions (104.7 MHz) as a result of fast exchange on the NMR time scale. As the Ni@Pb_{10}^{2-} sample is cooled, the line width of the Pb_{10} signal increases to 2310 Hz at −45 °C, which is interpreted as slowing intramolecular exchange on the NMR time scale. For comparison, the ^{207}Pb NMR signal of Ni@Pb_{12}^{2-} broadens only slightly from 240 Hz at 25 °C to 580 Hz at −45 °C. Since the Pb_{12} cluster has only a single Pb environment, the broadening in the later case can be attributed to chemical shift anisotropy associated with slow tumbling. We have yet to observe the limiting spectrum for Ni@Pb_{10}^{2-}.

Discussion

The M@Pb_{12}^{2-} (M = Pt, Pd, Ni) metal clusters are rare examples of naked metal icosahedra and, to our knowledge, are the only examples to be isolated as free ions in the solid state. They join the important class of gas-phase metallic icosahedra that include Al_{13}^{-1}, Au_{13}^{+1}, and Al@Pb_{12}^{-1} that are of great current interest both as free ions and in solid-state materials.[5,12,50] Importantly, isolation of the bulk crystalline salts shows that assembling naked metal clusters into three-dimensional ionic lattices is indeed possible. In particular, the $[K(2,2,2\text{-crypt})]_2[Pt@Pb_{12}]$ salt crystallizes a AlB_2-type lattice and serves as a prototype for assembled cluster materials made from naked metal clusters. In this lattice, the $[K(2,2,2\text{-crypt})]^+$ ions form hexagonal nets above and below the Pt@Pb_{12}^{2-} icosahedra (Figure 1) that is directly analogous to the graphite-like B_6 rings that coordinate to Al in AlB_2.[51] Similar packing has been seen in Schnöckel's $[Al_{77}\{N(SiMe_2)_2\}_{20}]^{2-}$ clusters[52] and, more recently, in the binary nanocrystal superlattices (BNSLs) comprising PbS (6.7 nm) and Pd (3.0 nm) particles in a 1:2 self-assembled composite.[53] Due to the spherical nature of the constituent particles, the (PbS−NP)(Pd−NP)$_2$ and related BNSLs show small-angle electron diffraction patterns that reflect the *P*6/*mmm* crystal symmetry of the parent AlB_2 lattice. In the present $[K(2,2,2\text{-crypt})]_2[Pt@Pb_{12}]$ salt, the crystal symmetry is lowered to $P\bar{3}$ due to the lack of mirror symmetry in the Pt@Pb_{12}^{2-} cluster and a slight puckering of the six-membered rings of $[K(2,2,2\text{-crypt})]^+$ ions, but the packing is clearly of the AlB_2 type. *Importantly, these systems illustrate the striking similarities of BNSLs and assembled cluster materials made*

(49) Wilson, W. L.; Rudolph, R. W.; Lohr, L. L.; Taylor, R. C.; Pyykko, P. *Inorg. Chem.* **1986**, *25*, 1535.
(50) Fassler, T. F.; Hoffmann, S. D. *Angew. Chem., Int. Ed.* **2004**, *43*, 6242.
(51) Wells, A. F. *Structural Inorganic Chemistry*, 5th ed.; Oxford University Press: New York, 1991.
(52) Ecker, A.; Weckert, E.; Schnockel, H. *Nature* **1997**, *387*, 379.
(53) Shevchenko, E. V.; Talapin, D. V.; Murray, C. B.; O'Brien, S. *J. Am. Chem. Soc.* **2006**, *128*, 3248.

from ionic lattices in what many have described as "artificial atoms" in the "new periodic table".[54−58]

The observation of Pb_{12}^{2-} and Pb_{10}^{2-} in the gas phase identifies two highly anticipated[37] members of Zintl ions that have not been previously observed. It has been well established that the E_9^{4-} and E_9^{3-} clusters (E = Ge, Sn, Pb) are the primary anions present in solution when alkali salts of the group 14 elements are extracted into polar solvents.[29−31] Despite the predicted stability of other deltahedral group 14 polyanions, the Pb_5^{2-} ion[31] is the only other naked ion isolated or identified in this family, and it only forms under certain conditions. The formation of Pb_{12}^{2-} clusters in the current study requires extensive fragmentation/disproportionation of the Pb_9^{4-} precursor in solution. Since the $Pt@Pb_{12}^{2-}$ cluster forms in relatively high yield (∼60%), one can assume that the fragmentation is facile in solution and the Pb_{12} icosahedron becomes more stable under these conditions. Moreover, the LDI studies show that empty and filled Pb_{12}^{2-} and Pb_{10}^{2-} ions are stable and readily assemble in the gas phase. Since the cluster fragmentation and recombination is occurring in the gas phase, it is not obvious why Pb_9 clusters are not observed in the MS studies.

Experimental Section

General Data. All reactions were performed in a nitrogen atmosphere drybox (Vacuum Atmosphere Co.). The ^{207}Pb NMR and ^{195}Pt NMR spectra were recorded on a Bruker DRX500 Avance spectrometer operating at 104.5 and 107.5 MHz, respectively. The LDI-TOF MS studies were performed on a Kompact Maldi Axima-CFR instrument with a purged glovebag over the sample chamber. The system uses a nitrogen laser light at 337 nm with a 3 ns pulse width. Longitudinal relaxation time (T_1) for Pb nuclei was measured by inversion recovery experiment at 285 K on a Bruker DRX500 Avance spectrometer operating at 107.5 MHz. The pulse sequence for inversion recovery experiment is 180°−τ−90° acquisition. Data interpreted by the software program plotting $\mathbf{M_z}$ (magnetization vector on z axis) vs **t** (delay for inversion recovery), where $M_z = (1 - 2\exp(-t/T_1)M_0)$, ($M_0$ = magnetization at thermal equilibrium).[51] M_z has zero signal intensity at time $\tau_o = T_1 \ln 2 \approx 0.7T_1$. The T_1 measurements were repeated three times for 12 different **t** (**t** = 0.0001 s, 0.002 s, 0.005 s, 0.0008 s, 0.0009 s, 0.001 s, 0.0015 s, 0.002 s, 0.003 s, 0.005 s, 0.01 s, 0.1 s) with d_1 (relaxation delay) 2 s. The result was obtained as 1.5 ms with the 1.433×10^{-2} uncertainties. AMRAY 1820K scanning electron microscope with a potential of 20 kV was used for energy-dispersive X-ray (EDX) studies.

Chemicals. Melts of nominal composition K_4Pb_9 were made by fusion (at high temperature) of stoichiometric ratios of the elements. The chemicals were sealed in evacuated, silica tubes and heated carefully with a natural gas/oxygen flame. 4,7,13,16,21,24-Hexaoxa-1,10-diazobicyclo[8,8,8]hexacosane (2,2,2-crypt) was purchased from Aldrich. $Ni(COD)_2$, $Pd(PPh_3)_4$, and $Pt(PPh_3)_4$ were purchased from Strem. Anhydrous ethylenediamine (en) and dimethylformamide (DMF) were purchased from Fisher, vacuum distilled from K_4Sn_9, and stored under dinitrogen. Toluene was distilled from sodium/benzophenone under dinitrogen and stored under dinitrogen.

Synthesis. Preparation of [K(2,2,2-crypt)]$_2$[Pt@Pb$_{12}$]. In vial 1, K_4Pb_9 (80 mg, 0.039 mmol) and 2,2,2-crypt (59.6 mg, 0.156 mmol) were dissolved in en (∼2 mL) and stirred for ∼5 min, yielding a dark-green solution. In vial 2, $Pt(PPh_3)_4$ (49 mg, 0.039 mmol) was dissolved in tol (∼1 mL) yielding a pale-yellow solution. The solution from vial 2 was added dropwise to vial 1, and the mixture was stirred ∼2 h, yielding a reddish brown solution. The solution was then filtered through tightly packed glass wool. After 1 day, big, black crystals of [K(2,2,2-crypt)]$_2$[Pt@Pb$_{12}$] precipitated. Yield: ∼48 mg (∼60%). EDX analysis on the crystals showed the presence of Pb, K, Pt atoms. ^{207}Pb NMR (DMF) δ (ppm): 1780, $^1J_{Pt-Pb} \approx 3432$ Hz. ^{195}Pt NMR (DMF) δ (ppm): −4427, $^1J_{Pt-Pb} \approx 3445$ Hz. T_1 = 1.5 ms. LDI-TOF MS, m/z = 2271 $Pt@Pb_{10}^{1-}$; 2310 $Pt@Pb_{10}K^{1-}$; 2683 $Pt@Pb_{12}^{1-}$; 2720 $Pt@Pb_{12}K^{1-}$; 2076 Pb_{10}^{1-}; 2488 Pb_{12}^{1-}; 2528 $Pb_{12}K^{1-}$.

Preparation of [K(2,2,2-crypt)]$_2$[Pd@Pb$_{12}$]·tol. In vial 1, K_4Pb_9 (80 mg, 0.039 mmol) and 2,2,2-crypt (59.6 mg, 0.156 mmol) were dissolved in en (∼2 mL) and stirred for ∼5 min, yielding a dark-green solution. In vial 2, $Pd(PPh_3)_4$ (29 mg, 0.020 mmol) was dissolved in tol (∼1 mL), yielding a pale-yellow solution. The solution from vial 2 was added dropwise to vial 1, and the mixture was stirred ∼2 h, yielding a reddish brown solution. The solution was then filtered through tightly packed glass wool. After 2 days, dark-red crystals of [K(2,2,2-crypt)]$_2$[Pd@Pb$_{12}$] precipitated. Yield: ∼20 mg (∼30%). ^{207}Pb NMR (DMF, 15 °C) δ (ppm): 1520 ($\Delta_{1/2}$: 285 Hz). LDI-TOF MS, m/z = 2182 $Pd@Pb_{10}^{1-}$; 2220 $Pd@Pb_{10}K^{1-}$; 2592 $Pd@Pb_{12}^{1-}$; 2526 $Pd@Pb_{12}K^{1-}$; 2076 Pb_{10}^{1-}; 2486 Pb_{12}^{1-}; 2527 $Pb_{12}K^{1-}$.

Preparation of [K(2,2,2-crypt)]$_2$[Ni@Pb$_{12}$]· en and [K(2,2,2-crypt)]$_2$[Ni@Pb$_{10}$]. In a vial 1, K_4Pb_9 (50 mg, 0.024 mmol) and 2,2,2-crypt (37.2 mg, 0.096 mmol) were dissolved in en (ethylenediamine) (∼2 mL), yielding a brown mixture. In vial 2, $Ni(COD)_2$ (10.9 mg, 0.024 mmol) was dissolved in tol (∼1 mL) producing a yellow solution. The contents of vial 2 were added to the contents of 1, and the reaction mixture was stirred for 2 h, yielding a dark red−brown solution. The reaction mixture was filtered through tightly packed glass wool in a pipet. Dark-red crystals formed in the reaction vessel after 4−5 days (∼25 mg, ∼90:10 mixture of $Ni@Pb_{10}^{2-}$: $Ni@Pb_{12}^{2-}$ crystals). ^{207}Pb NMR (DMF, 25 °C): δ (ppm): −996 ($\Delta_{1/2}$: 280 Hz) for $Pb_{10}Ni^{2-}$ and 1167 ($\Delta_{1/2}$: 240 Hz) for $Ni@Pb_{12}^{2-}$. LDI-TOF MS, m/z = 2135 $Ni@Pb_{10}^{1-}$; 2174 $Ni@Pb_{10}K^{1-}$; 2544 $Ni@Pb_{12}^{1-}$; 2584 $Ni@Pb_{12}K^{1-}$; 2076 Pb_{10}^{1-}; 2486 Pb_{12}^{1-}; 2527 $[Pb_{12}K]^{1-}$.

DFT Studies. The program package PRIRODA[42,43] was used for all DFT calculations with specifically functional PBE. Relativistic Stevens−Bausch−Krauss (SBK) effective core potentials were used in PBE calculations. A 311 split basis set was used for main group elements. The X-ray diffraction data of the $Ni@Pb_{10}^{2-}$ anion and $Pt@Pb_{10}^{2-}$ anion are used as starting coordinates for metalated and nonmetalated Pb_{10}^{2-} and Pb_{12}^{2-} anions, respectively. Coordinates used for bond order and charge calculations were first optimized by the PRIRODA program without constraints on symmetry. A multiplicity of 1 was used for the anions for convergence to occur. Analysis of the vibrational modes of the minimized structures showed no imaginary frequencies.

Crystallographic Studies. (1) [K(2,2,2-crypt)]$_2$[Pt@Pb$_{12}$]. A dark crystal was placed and optically centered on the Bruker SMART CCD system at −100 °C. The initial unit cell was indexed using a least-squares analysis of a random set of reflections collected from three series of 0.3° wide ω-scans, 10 s per frame, and 25 frames per series that were well distributed in reciprocal space. Data frames were collected [Mo Kα] with 0.3° wide ω-scans, 30 s per frame, and 606 frames per series. Five complete series were collected with a crystal-to-detector distance of 4.967 cm, thus providing a complete sphere of data to $2\theta_{max} = 50.0°$. A total of 16520 reflections were collected and corrected for Lorentz and polarization effects and absorption using Blessing's method as incorporated into the program, SADABS.

The SHELXTL program package was implemented for data processing, structure solution, and refinement. System symmetry, lack of systematic absences, and intensity statistics indicated the unique centric trigonal space group $P\bar{3}$ (no. 147) or the chiral $P3$ (no. 143). The

(54) Kiely, C. J.; Fink, J.; Brust, M.; Bethel, D.; Schiffrin, D. J. *Nature* **1998**, *396*, 444.
(55) Redl, F. X.; Cho, K.-S.; Murray, C. B.; O'Brien, S. *Nature* **2003**, *423*, 968.
(56) Saunders: A. E.; Korgel, B. A. *ChemPhysChem.* **2005**, *6*, 61.
(57) Shevchenko, E. V.; Talapin, D. V.; O'Brien, S.; Murray, C. B. *J. Am. Chem. Soc.* **2005**, *127*, 8741.
(58) Shevchenko, E. V.; Talapin, D. V.; Rogach, A. L.; Kornowski, A.; Haase, M.; Weller, H. *J. Am. Chem. Soc.* **2002**, *124*, 11480.

structure was determined by direct methods (XS) in $P\bar{3}$ with the successful location of nearly all non-hydrogen atoms. A single difference Fourier map was performed to locate the remaining non-hydrogen atoms. The final structure was refined to convergence [$\Delta/\sigma \leq 0.001$] with $R(F) = 7.30\%$, $wR(F^2) = 9.59\%$, GOF = 1.055 for all 2022 unique reflections [$R(F) = 3.52\%$, $wR(F^2) = 8.25\%$ for those 1434 data with $F_o > 4\sigma(F_o)$]. The final difference Fourier map possessed several peaks as large as 2.16 eÅ^{-2} close to the heavy atoms but was otherwise featureless, indicating that the structure is both correct and complete.

(2) [K(2,2,2-crypt)]$_2$[Pd@Pb$_{12}$]·Toluene. An orange plate was placed and optically centered on the Bruker SMART CCD system at −100 °C. The initial unit cell was attempted as described above but was unsuccessful because all of the crystals examined were twinned. The best scatterer was chosen for data collection. The relative contributions from the two twin components were determined using several data collection series. Nine hundred and ninety-nine reflections were randomly chosen via a thresholding routine, and these reflections were input into GEMINI to determined the initial twin relationship between the two components. Cellnow was implemented to better determine the orientation matrixes for the two twin components, orient the system correctly, and output a useable multiple matrice input file for SAINT. The twin matrixes corresponding to both components were input into SAINT, and the data were processed. At the completion of the run, the optimized merged matrix was re-input, and the data were processed a second time. This cyclic procedure was implemented for a total of five times. Twinabs was implemented to generate the HKLF5 file, and Strip_redV128 was used to remove redundant and "bug" reflections. Euhedral was implemented to further optimize the absorption correction.

The major component was used for structure determination. The SHELXTL program package was implemented to determine on the basis of intensity statistics and lack of systematic absences the centrosymmetric triclinic space group $P\bar{1}$ (no. 2). The structure was determined by direct methods using the program XS and refined using the program XL. All of the atoms were refined anisotropically. Hydrogen atoms were initially placed in calculated positions. All of the carbon atoms of the toluene molecule were refined with ISOR instructions. The final structure was refined to convergence [$\Delta/\sigma \leq 0.001$] with $R(F) = 10.14\%$, $wR(F^2) = 16.71\%$, GOF = 0.996 for all 17424 unique merged reflections [$R(F) = 5.96\%$, $wR(F^2) = 15.60\%$ for those 10936 data with $F_o > 4\sigma(F_o)$]. A final difference Fourier map possessed several peaks as large as 2.62 eÅ^{-3} near the heavy atoms, while the remainder of the map was featureless, indicating that the structure is therefore both correct and complete.

(3) [K(2,2,2-crypt)]$_2$[Ni@Pb$_{10}$]. A black plate with was placed and optically centered on the Bruker SMART CCD system at −100 °C. The initial unit cell was attempted using, but a minor twin component was present in all crystals examined. Data collection, correction, and deconvolution were performed as described above for [K(2,2,2-crypt)]$_2$-[Pd@Pb$_{12}$]. The SHELXTL program package was implemented to determine on the basis of intensity statistics and systematic absences the centrosymmetric monoclinic space group $C2/c$ (no. 15). The structure was determined by direct methods using the program XS. Refinement of the structure was achieved using the program XL. A majority of the atoms were refined anisotropically. Hydrogen atoms were placed in calculated positions throughout the refinement process. The final structure was refined to convergence [$\Delta/\sigma \leq 0.001$] with $R(F) = 8.27\%$, $wR(F^2) = 17.64\%$, GOF = 1.060 for all 5758 merged reflections [$R(F) = 5.82\%$, $wR(F^2) = 16.45\%$ for those 4234 data with $F_o > 4\sigma(F_o)$]. A final difference Fourier map possessed many large peaks, as large as 3.06 eÅ^{-3}, that were initially refined but found to have near zero occupancy and therefore considered "ghosts", while the remainder of the map was featureless, indicating that the structure is therefore both correct and complete.

(4) [K(2,2,2-crypt)]$_2$[Ni@Pb$_{12}$]·en. A black plate was placed and optically centered on the Bruker SMART1000 CCD system at −100 °C. The crystals were exceedingly air sensitive and did not diffract well, and only one successful set of data was collected. Several crystals were attempted but all possessed the same disorder pattern; thus, a small representative crystal was chosen. Data collection, correction, and deconvolution were performed as described above for [K(2,2,2-crypt)]$_2$[Pd@Pb$_{12}$]. The SHELXTL program package was implemented and indicated the centrosymmetric triclinic space group $P\bar{1}$(no. 2). The structure was determined by direct methods using the program XS. The two components were determined to exist with a ratio of 0.697: 0.303. Refinement of the structure was achieved using the program XL. A heavily disordered molecule of interest was located along with two potassium cryptand molecules and one multiply disordered ethylenediamine molecule. Many of the non-hydrogen atoms were refined anisotropically. Hydrogen atoms were placed in calculated positions during the final the refinement process. The final structure was refined to convergence [$\Delta/\sigma \leq 0.001$] with $R(F) = 16.82\%$, $wR(F^2) = 30.03\%$, GOF = 1.033 for all 7533 reflections [$R(F) = 10.31\%$, $wR(F^2) = 27.58\%$ for those 4281 data with $F_o > 4\sigma(F_o)$]. A final difference Fourier map possessed many large peaks near and within the NiPb$_{12}$ unit, while the remainder of the map was featureless, indicating that the structure is therefore essentially complete.

Acknowledgment. We are grateful to Noel Whittaker for assistance with the MS studies and Dr. Peter Zavalij for helpful discussions. We are extremely grateful to Prof. A. Vedernikov for help and guidance with the DFT calculations. This material is based upon work supported by the National Science Foundation under Grant No. 0401850.

Supporting Information Available: CIF files for the four crystal structures reported, selected bond distances and angles for the M@Pb$_{12}^{2-}$ clusters, full tables of distances from DFT calculations, and mass spectrometry data for the six compounds reported. This material is available free of charge via the Internet at http://pubs.acs.org.

JA061842M